

Transition state theory characterizes thin film macrospin dynamics driven by an oscillatory magnetic field: Inertial effects

Michael Maihöfer^a, Johannes Reiff^a, Jörg Main^a, Rigoberto Hernandez^{b,c,*}

^a Institut für Theoretische Physik I, Universität Stuttgart, 70550 Stuttgart, Germany

^b Department of Chemistry, Johns Hopkins University, Baltimore, Maryland 21218, USA

^c Departments of Chemical & Biomolecular Engineering, and Materials Science and Engineering, Johns Hopkins University, Baltimore, Maryland 21218, USA

Abstract

Understanding the magnetization switching process in ferromagnetic thin films is essential for many technological applications. We investigate the effects of periodic driving via magnetic fields on a macrospin system under explicit consideration of inertial dynamics. This is usually achieved by extending the Landau–Lifshitz–Gilbert equation with a term including the second time derivative of the magnetization. The dynamics of the magnetization switching can then be characterized by its switching rate. We apply methods from transition state theory for driven systems to resolve the rate of magnetization switching in this general case. In doing so, we find that magnetization exhibits resonance-like behavior under certain driving conditions, and it can be affected strongly by the system’s relaxation rate.

Keywords: magnetization switching, ferromagnetic thin film, Landau–Lifshitz–Gilbert equation, transition state theory, normally hyperbolic invariant manifold, stability analysis

1. Introduction

Single-domain nanomagnets have been studied extensively, in part because of their potential use in magnetic storage devices such as magnetoresistive random access memories (MRAMs) [1]. These applications in spintronics require control over the magnetization switching process in a ferromagnetic thin film. The application of a step function change in a static magnetic field is perhaps the simplest way to flip or drive the magnetization of a magnetic device. Stoner and Wohlfarth [2] characterized the corresponding magnetic model while also allowing for uniaxial anisotropy, and it is now well understood [3, 4]. Although such static magnetic fields can be used to drive macrospins, they tend to be quite large and thus attention has recently shifted towards more elaborate switching strategies to minimize energy requirements. For example, microwave-assisted switching [5–9] has been employed successfully by several groups, where alternating magnetic fields perpendicular to the easy axis are used to excite the precession of the magnetic moment. Such steps or pulses in the magnetic fields facilitate magnetization switching along the easy axis [10–13]. Control of magnetization switching has also been achieved using rotating radio-frequency fields perpendicular to the easy axis [14, 15].

In this paper, we focus on the macrospin dynamics driven by a single alternating field along the easy axis in the absence of any static external fields. Magnetization switching requires the crossing of the energy barrier separating two potential wells corresponding to *spin up* and *spin down*, respectively. We report the consequences on macrospins after their magnetization has been lifted near the barrier region but the flip has not yet occurred. This barrier gives rise to invariant manifolds that determine the switching behavior and are directly linked to the switching rate between the two potential wells. Using a harmonic driving field, the dynamics near the barrier can be modified to yield different switching rates. The dynamics of such systems is usually described by the Landau–Lifshitz–Gilbert (LLG) equation, which has only a two-dimensional phase space.

*Corresponding author

Email address: r.hernandez@jhu.edu (Rigoberto Hernandez)

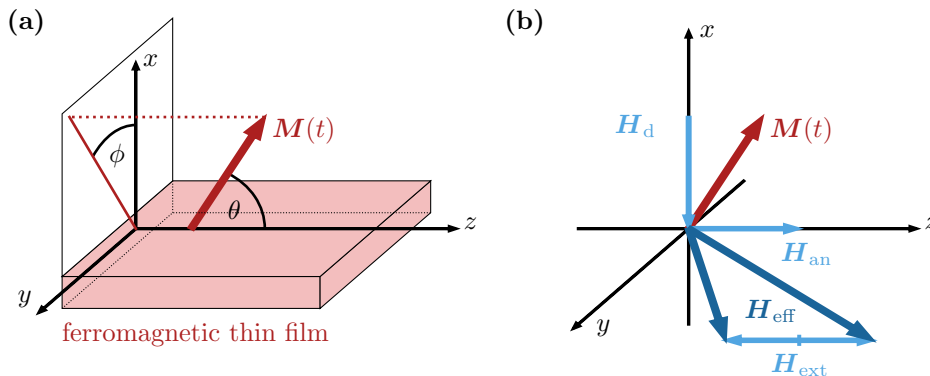


Figure 1: Schematic of (a) a ferromagnetic thin film with time-dependent, uniform magnetization $\mathbf{M}(t)$ and (b) magnetic field components acting on the magnetization. The magnetic field \mathbf{H}_{eff} in the ferromagnetic thin film consists of a demagnetizing field \mathbf{H}_d , an anisotropy field \mathbf{H}_{an} , and an external driving field \mathbf{H}_{ext} . The latter is shown as a double-arrow indicating its time-periodic oscillation around zero. The calculations are carried out in standard spherical coordinates with θ being the angle between \mathbf{M} and the z -axis, and ϕ being the angle in the xy -plane relative to the x -axis.

Some of us used the LLG equation within a transition state theory (TST) framework previously to reveal the phase space dynamics near the energy barrier and to obtain rates for magnetization switching when the inertia is neglected [16]. Without driving, the macrospins can be described by the invariant manifold of the transition state (TS), and the stability of those spins on the TS is quantified by the decay rate of macrospins in their vicinity. In a driven system, such as when torque is exerted on the macrospin by an oscillatory field, this manifold is time dependent, but can nevertheless be characterized. Here, we show that the associated decay rate can be computed using the methods of nonequilibrium TST [17, 18], even when inertial terms are included. For simplicity, we consider only the case when the torque exerted by the oscillatory field is in the direction of the easy axis.

In chemical reaction theory and more general activated dynamics problems [19], TST has been established as a useful, though often approximate, approach for calculating reaction rates. It has been adopted to non-chemical problems, such as atomic physics [20], solid state physics [21], cluster formation [22, 23], diffusion dynamics [24, 25], and cosmology [26–28]. TST approaches have been used previously by other groups [29, 30] to calculate the thermal stability of magnetic states. As we noted above, a time-dependent TST can also provide decay rates under the influence of an external oscillating driving field [16]. We extend these considerations here to address the magnetic moment in a periodically oscillating magnetic field using an extension of TST for driven systems when considering inertia. In particular, we found that an external driving’s amplitude and frequency can influence these properties.

In this paper, we now consider the LLG equation extended by an inertial term [31, 32], which has proven [33, 34] to describe the magnetization dynamics at picosecond time scales. From the dynamical point of view, the inclusion of inertia introduces a four-dimensional phase space which can give rise to added complexity. The extended model also features an additional material parameter, the relaxation time τ , that can influence the rates and phase space dynamics as a function of the driving parameters. Here, we focus on the case of sufficiently large τ to ensure that the governing differential equations remain second order. We further reveal the effects of a harmonic driving field on the rate of magnetization switching via a statistical approach using TST.

We start by introducing the thin-film model system of Fig. 1(a) in Sec. 2.1. A brief overview of TST in the context of the magnetization switching problem is provided in Sec. 2.2, including an overview of numerical methods implemented in this framework. We demonstrate in Sec. 3.1 that TST can be applied to uniformly magnetized systems. The results of our TST-based analysis are reported in Secs. 3.2 and 3.3.

2. Methods and materials

2.1. Inertial terms in the driven thin-film model

We previously used the Gilbert equation [35–37] to describe magnetization while ignoring the inertial term [16]. This is justified as long as the macrospin dynamics are not too fast. However, inertial effects play an important role for fast spin dynamics on a time scale of the order or below picoseconds [34]. While the Gilbert equation of motion

accounts for precession (in the first term) and damping (in the second term), inclusion of inertial effects [31, 32] manifests itself as a third term in the extended equation

$$\dot{\mathbf{m}} = -\gamma \mathbf{m} \times \mathbf{H}_{\text{eff}} + \alpha \mathbf{m} \times \dot{\mathbf{m}} + \alpha \tau \mathbf{m} \times \ddot{\mathbf{m}}, \quad (1)$$

where the unit vector $\mathbf{m}(t)$ is the evolution of the direction of magnetization whose magnitude is M_S , the parameter γ is the gyromagnetic factor, α is a non-dimensional damping parameter, τ is the relaxation time, and $\mathbf{H}_{\text{eff}} = \mathbf{H}_d + \mathbf{H}_{\text{an}} + \mathbf{H}_{\text{ext}}$ (cf. Fig. 1). In turn, the effective magnetic field can be written as the gradient of the free-energy potential U , i. e., $\mathbf{H}_{\text{eff}} = -(1/M_S) \nabla_{\mathbf{m}} U$. Curiously Eq. (1) arises not just from the framework of the breathing Fermi surface model [32, 38, 39], but also from a complementary non-equilibrium thermodynamics approach [31]. It has also been benchmarked through a ferromagnetic resonance experiment [33].

Here, we use the free energy [40, 41] of a ferromagnetic single-domain layer with a time-dependent but uniform magnetization. In the following, such a layer will be referred to as a *thin film* with uniform magnetization $\mathbf{M}(t)$, cf. Fig. 1. This model includes the uniaxial anisotropy field \mathbf{H}_{an} , the demagnetization field \mathbf{H}_d inducing a shape anisotropy, and the external driving \mathbf{H}_{ext} of an infinite thin film. The free-energy potential can be written as

$$U(\mathbf{m}, t) = -\frac{1}{2} H_K M_S m_z^2 + \frac{1}{2} M_S^2 m_x^2 - M_S H \sin(\omega t) m_z, \quad (2)$$

where the easy axis of the magnetic material lies in z -direction, and the thin film lies in the yz -plane. Here, $H_K = |\mathbf{H}_{\text{an}}|/m_z$ is the anisotropy field, and H and ω are the amplitude and frequency of the external driving field \mathbf{H}_{ext} , respectively. While we recognize that the thin film is small enough to accommodate macrospins, we approximate the shape anisotropy using the form for an infinitely extended thin film for simplicity. This approximation amounts to ignoring the relative contribution of m_z^2 from shape anisotropy, which in the current case is small compared to the leading term in the potential, or which in any case amounts to a rescaling of the coefficients of the squared magnetization component terms. Hence the potential includes only the additional term in m_x^2 to account for shape anisotropy. Figure 2(a) shows the potential from Eq. (2) in spherical coordinates at $t = 0$, where the spin up state corresponds to the region around $\theta = 0$ and the spin down state to $\theta = \pi$. For $t = 0$ there is a rank-1 saddle point at $\theta = \phi = \pi/2$, which oscillates periodically around this position over time. Figure 2(b) shows an example trajectory obtained from the equation of motion (1) and the potential from Eq. (2).

Equation (1) can be written explicitly as

$$\tau \ddot{\mathbf{m}} = -\frac{1}{\alpha} \mathbf{m} \times \dot{\mathbf{m}} - \frac{\gamma}{\alpha} \mathbf{m} \times (\mathbf{m} \times \mathbf{H}_{\text{eff}}) - \dot{\mathbf{m}} - \tau \dot{\mathbf{m}}^2 \mathbf{m} \quad (3)$$

for $\tau > 0$, and as the LLG equation

$$\dot{\mathbf{m}} = -\frac{\gamma}{1 + \alpha^2} \mathbf{m} \times \mathbf{H}_{\text{eff}} - \frac{\gamma \alpha}{1 + \alpha^2} \mathbf{m} \times (\mathbf{m} \times \mathbf{H}_{\text{eff}}) \quad (4)$$

for $\tau = 0$. The important difference between Eqs. (3) and (4) is that the inertial term completely changes the phase space structure of the macrospin dynamics. Without inertial effects, the LLG equation (4) is a first-order differential equation for the dynamics of the magnetic moment on a sphere, i. e., there are no independent velocities or momenta. In such a case, we have a two-dimensional phase space described by the angles (θ, ϕ) for the orientation of the macrospin. When applying TST to the magnetization switching process, θ is the *reaction coordinate* and ϕ formally plays the role of a momentum coordinate [16]. However, with inertial effects, the macrospin velocity in the second-order differential equation (3) must be taken into account. It extends the phase space from two to four dimensions described by angles and angular velocities $(\theta, \phi, v_\theta, v_\phi)$. As a consequence, the limit of small $\tau \lesssim 1$ in Eq. (1) becomes non-trivial due to the discontinuous change of the phase-space dimension. Thus formally and numerically, the two-dimensional phase space is appropriate for $\tau = 0$ —i. e., without inertial effects— as addressed in Ref. [16], and the four-dimensional phase space is valid for sufficiently strong inertial effects when $\tau \gtrsim 1$.

For the numerical calculations, we use units where $\gamma = 1$ and $M_S = 1$. This corresponds to $(\gamma M_S)^{-1}$ and M_S as the units of time t and magnetic field H , respectively. In these units, we set parameters

$$\alpha = 0.01, \quad \tau = 20, \quad \text{and} \quad H_K = 0.5 \quad (5)$$

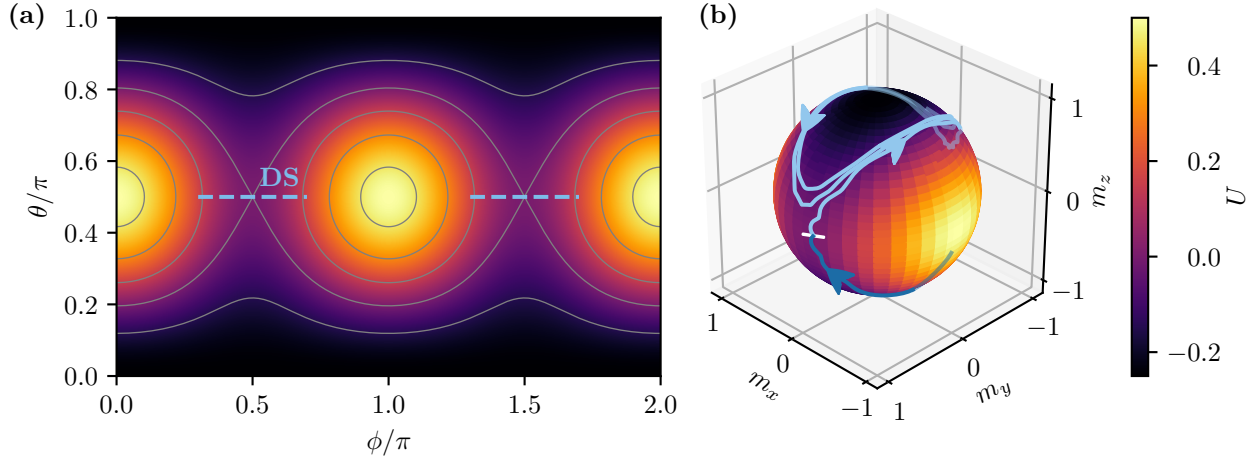


Figure 2: (a) Free-energy potential $U(\mathbf{m})$ from Eq. (2) at $t = 0$. In this representation, the spin-down state is at the bottom and the spin-up state is at the top, and separated by a naive dividing surface (DS)—shown as a dashed line—located horizontally at $\theta = \pi/2$. The potential exhibits two rank-1 saddle points at $(\phi, \theta) = (\pi/2, \pi/2)$ and $(3\pi/2, \pi/2)$. (b) Example trajectory for $\tau = 20$ and $H = 0$. For the reference system in Eq. (6), the potential difference between the saddle point and the minimum corresponds to $\Delta U = 3.14 \times 10^5 \text{ J m}^{-3}$ and relaxation time $\tau = 90.21 \text{ ps}$. The trajectory is initialized at $\theta = 0.5\pi$, $\phi = 0.55\pi$, and $v_\theta = v_\phi = -0.049$ (white line segment) near the saddle point that separates spin-up and spin-down states. The trajectory is propagated in both forward and backward time direction. Arrow heads on the trajectory indicate the direction of time. The trajectory is drawn with a lighter shade in forward direction (spin-up state) and with a darker shade in backward direction (spin-down state). Transitions between the two spin states are defined by the DS, which in this example is crossed near the initial point. For reference, a sphere of radius 0.98 indicates the free-energy potential $U(\mathbf{m})$. Semitransparency is used to indicate when the trajectory is on the back side of the potential sphere.

unless stated otherwise. For example, in the cases reported in Refs. [8, 13, 15], $\gamma = 2.217 \times 10^5 \text{ m A}^{-1} \text{ s}^{-1}$ and $M_S = 1 \times 10^6 \text{ A m}^{-1}$. Our parameters then take the values

$$\tau = 90.21 \text{ ps} \quad \text{and} \quad H_K = 5 \times 10^5 \text{ A m}^{-1} \quad (6)$$

in physical units while α stays dimensionless. The inclusion of inertia allows for a formal analogy to a classical spinning top, as pointed out in Refs. [42, 43]. In Lagrangian formulation, Eq. (3) can be written via the Lagrangian

$$\mathcal{L} = \frac{1}{2} \left(\alpha \tau \left[\dot{\phi}^2 \sin^2(\theta) + \dot{\theta}^2 \right] + \dot{\phi}^2 \cos^2(\theta) \right) - U(\theta, \phi), \quad (7)$$

which includes kinetic and potential energy terms, and the Rayleigh dissipation function

$$\mathcal{R} = \frac{\alpha}{2} \left[\dot{\phi}^2 \sin^2(\theta) + \dot{\theta}^2 \right]. \quad (8)$$

The equations of motion in Euler coordinates can be recovered using the Euler-Lagrange equation

$$\frac{d}{dt} \frac{\partial \mathcal{L}}{\partial \dot{q}_i} - \frac{\partial \mathcal{L}}{\partial q_i} + \frac{\partial \mathcal{R}}{\partial \dot{q}_i} = 0. \quad (9)$$

In terms of the spinning top, setting $\alpha = \tau = 0$ results in pure *precession*, where trajectories follow equipotential lines of the potential $U(\theta, \phi)$. Inclusion of damping—i. e., $\alpha \neq 0$ and $\tau = 0$ —leads to a damped precession converging towards the minimum of the potential. The further inclusion of inertia—i. e., $\alpha \neq 0$ and $\tau \neq 0$ —leads to additional *nutation* and the complex dynamics addressed in this paper.

2.2. Transition state theory

2.2.1. Adapting TST to macrospin decays

The model described in Sec. 2.1 features two metastable configurations along the z -direction. They are separated by a potential barrier oscillating around the xy -plane. Any flip between the magnetization states has to pass over the

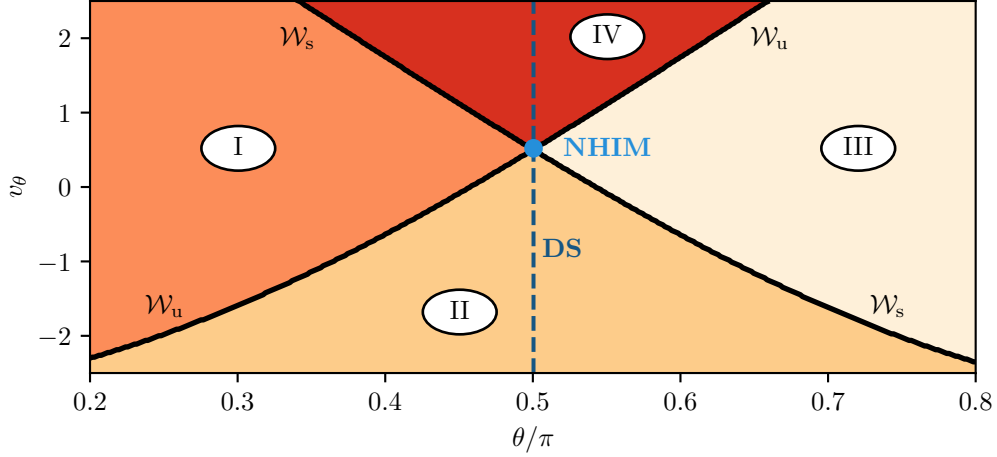


Figure 3: Stable and unstable manifolds (black lines) in a phase space section ($\phi = \pi/2$, $v_\phi = 0$) dividing the phase space into distinct regions (I)–(IV) (see text). The intersection of stable and unstable manifolds is the normally hyperbolic invariant manifold (NHIM, circle marker), which is the anchor for a DS (blue dashed) in v_θ -direction. Made for $\tau = 20$, $H = 0.15$, and $\omega = \pi/8$ at $t = 0$. For the reference parameters in Eq. (6) this corresponds to $\tau = 90.21$ ps, $H = 1.5 \times 10^5$ A m $^{-1}$, and $\omega = 0.547$ THz.

time-dependent energy barrier. A magnetization configuration is trapped or might flip depending on whether or not its energy is sufficient to pass through the rank-1 saddle point. The flipping rate is therefore highly dependent upon the dynamics of the phase space in the vicinity of the rank-1 saddle. The question of reaction rates between such metastable configurations arises frequently in chemical reactions, where TST has been established to calculate these reaction rates [44–48]. Recent work [17, 49–53] has addressed the use of TST for driven chemical reactions which is applied here to address the driven magnetization switching problem.

Given a potential energy function and an equation of motion, TST is concerned with constructing a recrossing-free DS separating spin-down and spin-up basins in phase space. The rate is then calculated by the directional flux through the DS. The resulting instantaneous decay rate is

$$k(t) = -\frac{\dot{N}(t)}{N(t)}, \quad (10)$$

where $N(t)$ is the time-dependent reactant population. In the original formulation, the DS was fixed, planar and orthogonal to the reactive direction. While a useful approximation, it overestimates the rates because of recrossings and neglect of the stochastic forces.

2.2.2. Normally hyperbolic invariant manifolds for macrospins

A major advance in improving TST has arisen from the identification of geometric properties of the phase space to generalize the DS through the association of the rank-1 saddle point with a normally hyperbolic invariant manifold (NHIM) [54–60]. This $(2d - 2)$ -dimensional manifold consists of all trajectories trapped forever in the saddle point region. In the following, these trajectories will be referred to as *TS trajectories*. It is complemented by the $(2d - 1)$ -dimensional stable and unstable manifolds \mathcal{W}_s and \mathcal{W}_u consisting of trajectories converging to the NHIM for $t \rightarrow \infty$ and $t \rightarrow -\infty$, respectively. Figure 3 shows a two-dimensional cut of the magnetization’s four-dimensional phase space, reducing stable and unstable manifold to a line and the NHIM to a point. The stable and unstable manifolds divide the phase space into four distinct regions, where (I) the spin stays up, (II) the spin flips from down to up, (III) the spin stays down, and (IV) the spin flips up to down. A recrossing-free DS must only slice through the regions (II) and (IV), and thus has to be anchored at the NHIM.

The problem of constructing a recrossing-free DS thus reduces to finding the NHIM. Different numerical algorithms exist for this task, e. g., those based on Lagrangian descriptors and variants thereof [17, 61–63]. Here, we choose the binary contraction method (BCM): Any initial point can be classified numerically using an interaction region around the saddle, where trajectories leaving it are clearly classified as either spin-up or spin-down configurations. This

region does not necessarily have to be defined via the unstable direction of the saddle (i. e., θ) as long as it enables a clear classification. In practice, we found that choosing $\phi \in [0.1\pi, 0.9\pi]$ allowed such classification. The resulting binary classification can be performed for the forward and backward time direction, thus yielding the four distinct regions (I)–(IV) introduced above. Since the NHIM is of codimension 2, the phase space can always be reduced to an effectively two-dimensional problem using cuts transverse to the NHIM, as illustrated in Fig. 3.

Several numerical approaches for using the NHIM to calculate rates are now available: the ensemble method [51, 52, 64], the Floquet method [65], and the local manifold analysis (LMA) [28, 51]. Conceptually, all of these methods work by initializing an appropriate ensemble on one side of the DS and counting the number of crossings over time. The methods, however, differ significantly in the way the ensemble is modeled mathematically and propagated computationally. In the cut shown in Fig. 3, the NHIM is a point of intersection at the closure of all four regions, and is obtained here, and throughout the present work, using the BCM [66].

2.2.3. Decay rates between macrospin states

There exist various methods for determining the decay rate of a TS trajectory Γ_0 . In this paper, we adopt the LMA because we had found earlier that it provides a good compromise between computational efficiency and the extent of data that it readily provides. The computationally expensive step is usually the propagation of many individual states through the DS. For sufficiently smooth manifolds and a linear DS along the reactive velocity (as satisfied in the problems addressed here), the propagation can be replaced by an analytical calculation revealing the stability of the system near the NHIM. In the following, without loss of generality, we choose coordinates such that the TS trajectory Γ_0 is always located at the origin. Furthermore, we assume that the DS is parallel to the v_θ -axis, cf. Fig. 3.

Specifically, we first obtain the Jacobian

$$\mathbf{J} = \frac{\partial(\dot{\theta}, \dot{\phi}, \dot{v}_\theta, \dot{v}_\phi)}{\partial(\theta, \phi, v_\theta, v_\phi)} \quad (11)$$

for the four-dimensional phase space of the equations of motion with $v_\theta = \dot{\theta}$ and $v_\phi = \dot{\phi}$. Two of the eigenvectors of \mathbf{J} locally point in the direction of the stable and unstable manifolds while the other two are tangent to the NHIM. In the following calculations, we consider a $(\theta, v_\theta)^\top$ -section of phase space with fixed ϕ , v_ϕ and time t_0 . In this two-dimensional frame, the eigenvector pointing in the stable direction is $\tilde{\mathbf{F}}^s = (\theta^s, v_\theta^s)^\top$, while the eigenvector pointing in the unstable direction is $\tilde{\mathbf{F}}^u = (\theta^u, v_\theta^u)^\top$. We now consider an equidistant, linear ensemble on the reactant side, parameterized by

$$\tilde{\mathbf{I}}(a, t) = -\tilde{\mathbf{F}}^s(t) + a\tilde{\mathbf{F}}^u(t) \quad (12)$$

with $a \in [0, 1]$. The ensemble is initialized in a $(\theta, v_\theta)^\top$ -section of phase space with fixed bath coordinates ϕ and v_ϕ , and thus depends implicitly on these latter coordinates. The norms of the eigenvectors $\tilde{\mathbf{F}}^s(t_0)$ and $\tilde{\mathbf{F}}^u(t_0)$ at initial time t_0 are chosen such that $\tilde{\mathbf{I}}(1, 0) = \tilde{\mathbf{F}}^s(t_0) + \tilde{\mathbf{F}}^u(t_0)$ is located on the DS. The DS can be described by a normal vector $\tilde{\mathbf{n}} = (1, 0)^\top$ in the section of the ensemble. Furthermore, we define $\tilde{\mathbf{F}}^s(t)$ and $\tilde{\mathbf{F}}^u(t)$ as the time evolution of states initially located at $\tilde{\mathbf{F}}^s(t_0)$ and $\tilde{\mathbf{F}}^u(t_0)$, respectively.

The value of $a^{\text{DS}}(t)$, at which the ensemble pierces the DS, depends on the length of $\tilde{\mathbf{F}}^s(t)$ and $\tilde{\mathbf{F}}^u(t)$ and is initially $a^{\text{DS}}(t_0) = 1$. Since the number of reacted particles in the ensemble is proportional to a^{DS} , Eq. (10) becomes

$$k(t_0) = -\dot{a}^{\text{DS}}(t_0). \quad (13)$$

To determine $\dot{a}^{\text{DS}}(t_0)$ we use the fact that

$$\tilde{\mathbf{n}} \cdot \tilde{\mathbf{I}}(a^{\text{DS}}(t), t) \equiv 0 \quad (14)$$

by definition. Differentiating this identity relation with respect to time yields

$$\begin{aligned} 0 &= \tilde{\mathbf{n}} \cdot \frac{d}{dt} \tilde{\mathbf{I}}(a^{\text{DS}}(t), t) \\ &= \tilde{\mathbf{n}} \cdot \left[-\frac{d\tilde{\mathbf{F}}^s(t)}{dt} + \frac{da^{\text{DS}}(t)}{dt} \tilde{\mathbf{F}}^u(t) + a^{\text{DS}}(t) \frac{d\tilde{\mathbf{F}}^u(t)}{dt} \right] + \tilde{\mathbf{n}} \cdot \left[\frac{\partial \tilde{\mathbf{I}}(a^{\text{DS}}(t), t)}{\partial \phi} \frac{d\phi(t)}{dt} + \frac{\partial \tilde{\mathbf{I}}(a^{\text{DS}}(t), t)}{\partial v_\phi} \frac{dv_\phi(t)}{dt} \right]. \end{aligned} \quad (15)$$

Here, the $d\phi(t)/dt$ and $dv_\phi(t)/dt$ terms describe how the ensemble moves out of the initial plane during propagation. We can discard $a^{\text{DS}}(t)$ by evaluating Eq. (15) at time t_0 . Using $\theta^u = \theta^s$ and the linearized equation of motion $d\mathbf{\Gamma}/dt = \mathbf{J}\mathbf{\Gamma}$ in the full four-dimensional phase space, Eq. (15) can be rewritten as

$$\dot{a}^{\text{DS}}(t_0) = -J_{\theta, v_\theta} \frac{v_\theta^u - v_\theta^s}{\theta^u} + \frac{1}{\theta^u} \frac{d\theta^{\text{DS}}}{dt} \quad (16)$$

with $d\theta^{\text{DS}} = \tilde{\mathbf{n}} \cdot [(\partial\tilde{\mathbf{\Gamma}}/\partial\phi)d\phi + (\partial\tilde{\mathbf{\Gamma}}/\partial v_\phi)dv_\phi]$. The first term on the right hand side of Eq. (16) can be interpreted as the difference in the slopes of stable and unstable manifolds in the plane. The second term takes care of the ensemble drifting out of plane, i. e., the change of the position of the DS when changing the orthogonal modes ϕ and v_ϕ .

The resulting rate

$$k(\phi, v_\phi, t) = \frac{v_\theta^u - v_\theta^s}{\theta^u} - \frac{\theta^{\text{DS}}(t_0 + \delta t) - \theta^{\text{DS}}(t_0)}{\theta^u \delta t}, \quad (17)$$

once again, only depends on the difference of slopes v_θ/θ of the linearized stable and unstable manifolds in plane and the movement of the NHIM out of plane. For the numerical rate calculations in this paper, we first find trajectories on the NHIM using the methods described in Sec. 2.2.2. Given a specific point (ϕ, v_ϕ) on the NHIM at time t_0 , we calculate the difference of the stable and unstable manifolds' slopes $(v_\theta^u - v_\theta^s)/\theta^u$ in a two-dimensional phase-space cut transverse to the NHIM, i. e., the reaction coordinates θ and v_θ . A trajectory is propagated for time δt starting at the current location of the NHIM $(\theta^\ddagger, \phi, v_\theta^\ddagger, v_\phi)$ at time t_0 . Due to the definition of the DS, the change $\theta^\ddagger(t_0 + \delta t) - \theta^\ddagger(t_0)$ corresponds to the term $\theta^{\text{DS}}(t_0 + \delta t) - \theta^{\text{DS}}(t_0)$ in Eq. (17).

The parameters of the LLG equation enter the rate indirectly by specifying the exact geometry of the NHIM, and the stable and unstable manifolds.

3. Results

3.1. Application of TST

The inclusion of dissipation and gyroscopic effects creates additional challenges to the application of TST to magnetization switching [16].

Figure 2(b) shows a typical trajectory. The magnetization vector moves towards alignment with the z -axis. This trajectory approximately follows equipotential lines, with the Gilbert damping relaxing the trajectory to the minimum of the potential. The additional inertia creates nutation loops that can be seen as wiggles along the general path of the trajectory. In the forward and backward time direction, a typical trajectory loses and gains energy, respectively, in doing so. Thus the motion of the magnetization in the backward direction would lead to ever growing nutation loops.

We found that the dynamics of the magnetization satisfies the necessary assumptions for TST only when we consider cases in which the relaxation times exceed a certain threshold (here $\tau \gtrsim 1$, depending on the driving parameters). The reliable classification of trajectories into spin-up and spin-down domains is a central requirement for the numerical determination of the NHIM's position using the BCM. This is only possible when the dynamics is sufficiently dominated by a bottleneck that gives rise to a well-defined DS. For $\tau \lesssim 1$, however, we found that the predominant nutation circles do not admit such a structure or a clear classification as spin-up or spin-down states. The classification in backward time direction is impossible in this parameter regime, for example. Therefore, all of the structure of the reaction geometry and the associated rate calculations reported here are limited to cases in which the relaxation times are above the observed relaxation threshold ($\tau \gtrsim 1$), as noted in Section 2.1. For the purposes of this paper, this is not a significant limitation since recent studies [34] suggest relaxation times τ on the order of 2 to 20 when specified in the dimensionless units of this work.

3.2. Dynamics on the NHIM

For a system with $\tau = 0$ described by the standard LLG equation (4), the NHIM is a single trajectory. However, for $\tau > 0$, described by Eq. (3), the NHIM becomes a two-dimensional, time-dependent manifold, and therefore the dynamics on the NHIM needs to be considered in calculating the rate.

For any set of parameters, the dynamics on the NHIM can be visualized using Poincaré cuts. We found that any initial starting point on the NHIM will converge towards a single periodic trajectory on the NHIM over time due to

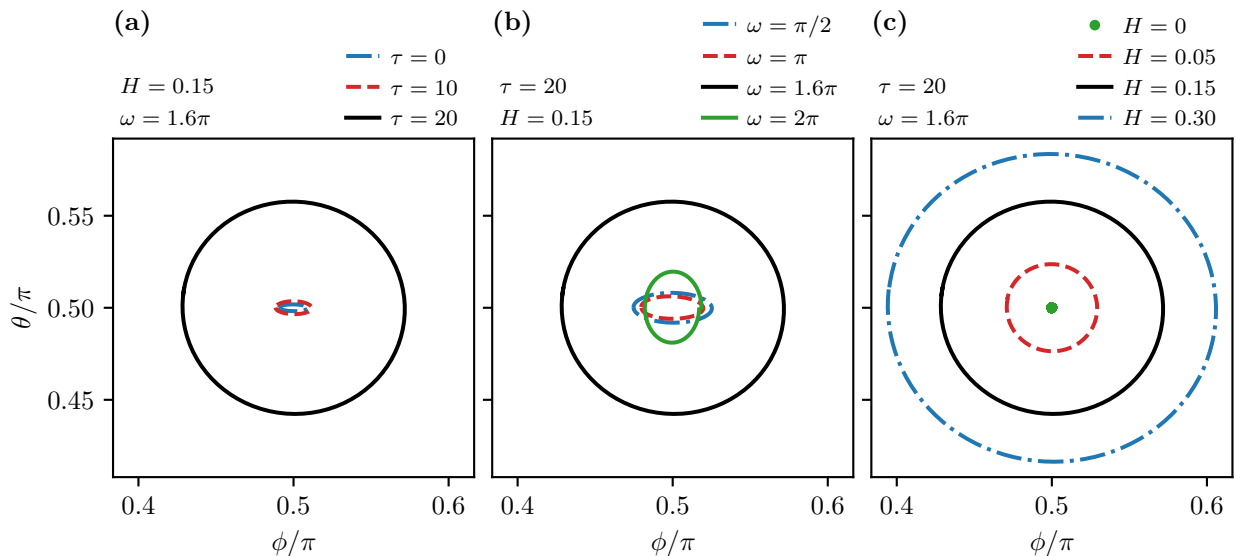


Figure 4: Periodic TS trajectories on the NHIM. We use a reference parameterization ($H = 0.15$, $\omega = 1.6\pi$, and $\tau = 20$) shown as a black solid curve in all three panels. For the reference system in Eq. (6), this corresponds to $H = 1.5 \times 10^5 \text{ A m}^{-1}$, $\omega = 7.0 \text{ THz}$, and $\tau = 90.21 \text{ ps}$. All other curves correspond to different parameterizations across the three panels. (a) At fixed $H = 0.15$ and $\omega = 1.6\pi$, the relaxation time τ is varied. The trajectory for $\tau = 0$ was determined via the standard LLG equation. (b) At fixed $\tau = 20$ and $H = 0.15$, the driving frequency ω is varied. (c) At fixed $\tau = 20$ and $\omega = 1.6\pi$, the driving amplitude H is varied.

the damping terms. Indeed, though not shown explicitly, across the parameter regimes observed in this work, none of the trajectories exhibited chaotic motion. The rate at which points on the NHIM converge towards this periodic trajectory scales approximately linearly with the inverse of the relaxation time τ . The resulting TS trajectory has the same frequency as the driving field. The amplitude of its motion depends on both the frequency and amplitude of the driving field. The frequency at which the amplitude of motion is maximal [34, 67] is approximately given by

$$\omega = \frac{\sqrt{1 + \alpha\tau\gamma H}}{\alpha\tau}. \quad (18)$$

Figure 4 shows the periodic TS trajectory for different sets of parameters. In Fig. 4(a), the relaxation time is varied at fixed driving frequency and driving amplitude. For most values of the relaxation time, the TS trajectory is close to the TS trajectory of the system without inertia. At $\tau = 20$, the resonant condition (18) is met and the trajectory exhibits a particularly large amplitude. In Fig. 4(b) the driving frequency is varied at fixed driving amplitude and relaxation time. The amplitude of the oscillation highly depends on the frequency. In the limit of low frequency, the TS trajectory converges towards the trajectory of the saddle point on the free-energy potential (2). In the limit of high frequency, the TS trajectory shrinks to a point. In the intermediate range, the TS trajectory exhibits resonant behavior, increasing the amplitude of the oscillation to a maximum. In Fig. 4(c) the driving amplitude is varied at fixed driving frequency and relaxation time. The amplitude of the oscillation increases strictly monotonically with driving amplitude.

3.3. Rates

We now calculate the instantaneous and average rates for magnetization switching associated with the TS trajectory. The instantaneous rates depend on time because they are evaluated at a time-dependent position relative to the time-dependent location of the TS while experiencing a time-dependent driving force; cf. Eq. (17).

We found, though not shown, that the rate over time is periodic with the driving field with twice the frequency of driving $\omega = 2\pi/T$ and an average value dependent on frequency and amplitude of the driving. This could have been expected because the rate over time depends on the geometry of the system's phase space along the trajectory

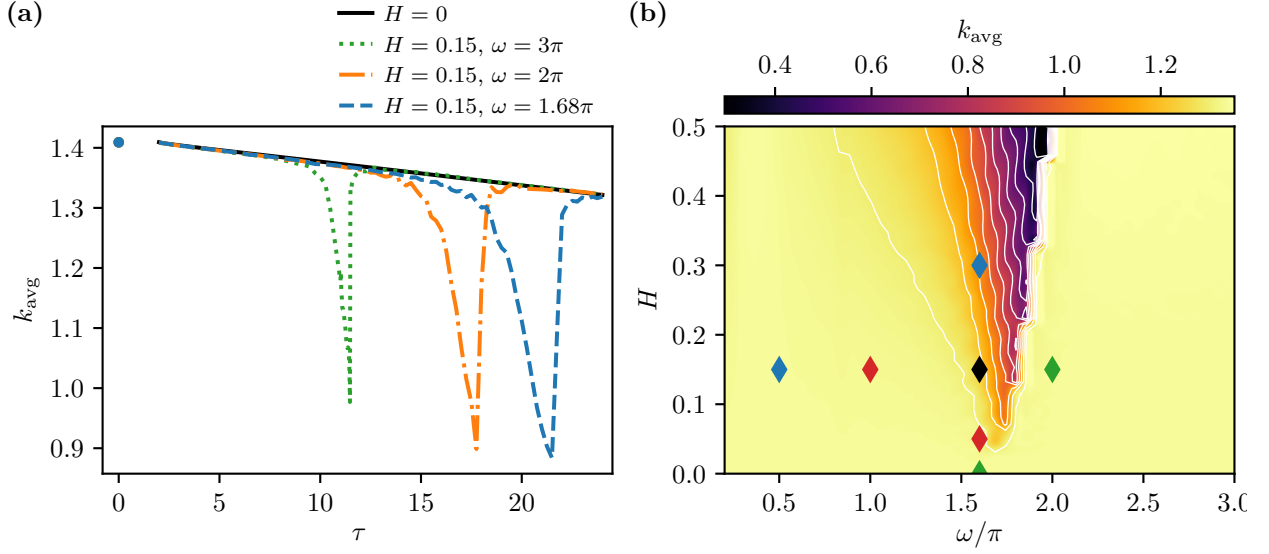


Figure 5: (a) Averaged rate k_{avg} as a function of relaxation time τ . Overlapping circle markers at $\tau = 0$ show rates determined via the standard LLG equation. (b) Averaged rate k_{avg} as a function of driving frequency ω and amplitude H at $\tau = 20$. The diamonds and their colors (or shades in print) at $H = 0.15$ and $\omega = 1.6\pi$ correspond to the TS trajectories in Figs. 4(b) and 4(c), respectively. The black diamond corresponds to $H = 1.5 \times 10^5 \text{ A m}^{-1}$, $\omega = 7.0 \text{ THz}$, and $\tau = 90.21 \text{ ps}$ for the system in Eq. (6).

that carries the DS. For the periodic TS trajectory, the rate is therefore periodic with the driving by construction. Furthermore, the system exhibits the invariance

$$\mathbf{H}_{\text{eff}}(\theta, \phi, t) \cdot \hat{\mathbf{e}}_j = -\mathbf{H}_{\text{eff}}(\pi - \theta, \pi - \phi, t + T/2) \cdot \hat{\mathbf{e}}_j, \quad (19)$$

where $\hat{\mathbf{e}}_j$ is one of the unit vectors $\hat{\mathbf{e}}_\theta$ or $\hat{\mathbf{e}}_\phi$. Together with the TS trajectory's related symmetry (cf. Fig. 4)

$$\mathbf{m}(\theta, \phi, t) = \mathbf{m}(\pi - \theta, \pi - \phi, t + T/2), \quad (20)$$

this imposes further constraints on the rate, forcing $k(t)$ to be periodic with twice the period of the driving. Similar observations have previously been made in other physical systems [16, 51, 64].

Figure 5(b) shows the averaged rate as a function of driving frequency and amplitude. The averaged rate is nearly constant for low frequencies. Nevertheless, the rate depends significantly on the features of the transition state trajectory in response to the driving. For a given ω , the average rate decreases with increasing H across the parameter space shown in Fig. 5(b). At driving frequencies approaching $\omega = 1.68\pi$, the rate reaches a minimum. A slight increase in the frequency results in a sharp increase of the rate as the driven rate converges on the static rate. The minimum of the potential thereby coincides with the resonance maximum of the periodic TS trajectory. At the frequency of the minimum of the rate, the transition state trajectory has a large amplitude, and thus explores a larger phase space region further away from the region around $\theta = \phi = \pi/2$. This connection is indicated by the diamonds in Fig. 5(b), whose location corresponds to the parameters of the external driving used in Figs. 4(b) and 4(c). The sharp increase in rate for incrementally larger frequency is accompanied by the abrupt decline of the TS trajectory's diameter.

Figure 5(a) shows the averaged rate over relaxation time. Without any external driving, the averaged rate decreases almost linearly with relaxation time. In the case of external driving, the rates stay close to the rate without driving for very low and high relaxation times. However, for each specified H and ω , there is a relaxation time τ where the rate is especially low as shown in Fig. 5(a). That resonance is also observed for a specific τ over the domain of ω and H , such as that seen in Fig. 5(b) for $\tau = 20$. The minima of the rate for different τ are determined by the resonant condition (18). Finally, Fig. 5(a) also shows that the rates for $\tau \rightarrow 0$ are consistent with the rates calculated using the standard LLG equation, which is equivalent to $\tau = 0$. This is numerically nontrivial due to the different dimensionalities of the phase space of the equation with and without inertia, and confirms the applicability and accuracy of our numerical TST implementation.

4. Conclusion and outlook

In this paper, we report the use of TST to calculate rates of magnetization switching in a model system considering inertial terms and under the influence of external driving fields. We employed a modified version of the LLG equation in a free-energy potential featuring a periodically driven rank-1 saddle as our model system. We used methods from TST to identify the NHIM and to calculate the rate of magnetization flips. We successfully identified the NHIM for cases with large relaxation times.

In this work, we confirmed the use of TST in the context of the macrospin problem by demonstrating that it recapitulates several known properties of driven macrospins. While the amplitude of spin trajectories is highly dependent on the amplitude and frequency of the driving, we find that the system did not exhibit chaotic behavior in the regimes considered here. Moreover, the NHIM contains a periodic orbit that allows us to characterize properties of the macrospin dynamics. For example, this periodic TS trajectory exhibits a resonance—i. e., a non-monotonic dependence of the width of the TS trajectory on the frequency of the driving—which might have been expected from prior work in the literature (cited above). Our results are also consistent with those obtained using the standard LLG equation in the limit of vanishing relaxation time. While this limiting result may be expected from a physical point of view, it is still an important indicator that the numerical implementation is correct because the equations with and without inertia correspond to phase spaces with a different number of dimensions.

We found that any initial point on the NHIM converges towards the periodic TS trajectory. This confirms that the TST structure is useful in identifying stable regions in the context of the decay of macrospins. While we did not find bifurcations in the rate over the parameter space explore here, we can conjecture their existence at more extreme conditions given our earlier findings in the context of chemical reactions [52, 68].

We also calculated the instantaneous rates along the periodic TS trajectory. These rates have twice the frequency as the external driving. Their values drop significantly at specific combinations in frequency and inertia when the periodic TS trajectory is in resonance. The inclusion of inertia therefore allows for richer dynamics on the NHIM due to increased dimensionality of the phase space with the inclusion of the momentum variables. Thus the average rate of magnetization switching exhibits complex responses to external driving in correspondence with the changing phase space structure of the TS trajectory that is only available through the use of the nonequilibrium TST formalism. The verification of this phenomenon is also a challenge that remains to be done. For practical applications, the inclusion of spin-transfer torque is relevant, and the TST formalism can be extended to include such effects. The investigation of such effects remains to be done.

Declaration of competing interest

The authors declare that they have no known competing financial interests or personal relationships that could have appeared to influence the work reported in this paper.

CRediT authorship contribution statement

Michael Maihöfer: Methodology, Software, Formal analysis, Investigation, Writing – Original Draft, Visualization. **Johannes Reiff:** Methodology, Software, Validation, Resources, Data Curation, Writing – Review & Editing, Visualization. **Jörg Main:** Conceptualization, Methodology, Formal analysis, Resources, Writing – Review & Editing, Supervision, Project administration, Funding acquisition. **Rigoberto Hernandez:** Conceptualization, Writing – Review & Editing, Supervision, Project administration, Funding acquisition.

Acknowledgments

Useful discussions with Robin Bardakcioglu are gratefully acknowledged. The German portion of this collaborative work was partially supported by the Deutsche Forschungsgemeinschaft (DFG) through Grant No. MA1639/14-1. The US portion was partially supported by the National Science Foundation (NSF) through Grant No. CHE 2102455. This collaboration has also benefited from support by the European Union’s Horizon 2020 Research and Innovation Program under the Marie Skłodowska-Curie Grant Agreement No. 734557.

References

- [1] C. Augustine, N. N. Mojumder, X. Fong, S. H. Choday, S. P. Park, K. Roy, Spin-transfer torque MRAMs for low power memories: Perspective and prospective, *IEEE Sens. J.* 12 (2012) 756–766. doi:10.1109/JSEN.2011.2124453.
- [2] E. C. Stoner, E. P. Wohlfarth, A mechanism of magnetic hysteresis in heterogeneous alloys, *Philos. Trans. R. Soc., A* 240 (1948) 599–642. doi:10.1098/rsta.1948.0007.
- [3] C. Tannous, J. Gieraltowski, The Stoner–Wohlfarth model of ferromagnetism, *Eur. J. Phys.* 29 (2008) 475–487. doi:10.1088/0143-0807/29/3/008.
- [4] C. Tannous, J. Gieraltowski, A Stoner–Wohlfarth model Redux: Static properties, *Physica B* 403 (2008) 3563–3570. doi:10.1016/j.physb.2008.05.031.
- [5] C. Thirion, W. Wernsdorfer, D. Mailly, Switching of magnetization by nonlinear resonance studied in single nanoparticles, *Nat. Mater.* 2 (2003) 524–527. doi:10.1038/nmat946.
- [6] J.-G. Zhu, X. Zhu, Y. Tang, Microwave assisted magnetic recording, *IEEE Trans. Magn.* 44 (2008) 125–131. doi:10.1109/tmag.2007.911031.
- [7] S. Okamoto, N. Kikuchi, M. Furuta, O. Kitakami, T. Shimatsu, Switching behaviors and its dynamics of a Co/Pt nanodot under the assistance of rf fields, *Phys. Rev. Lett.* 109 (2012) 237209. doi:10.1103/physrevlett.109.237209.
- [8] T. Taniguchi, Magnetization reversal condition for a nanomagnet within a rotating magnetic field, *Phys. Rev. B* 90 (2014) 024424. doi:10.1103/physrevb.90.024424.
- [9] H. Suto, T. Nagasawa, K. Kudo, K. Mizushima, R. Sato, Microwave-assisted switching of a single perpendicular magnetic tunnel junction nanodot, *Appl. Phys. Express* 8 (2015) 023001. doi:10.7567/apex.8.023001.
- [10] N. Barros, M. Rassam, H. Jirari, H. Kachkachi, Optimal switching of a nanomagnet assisted by microwaves, *Phys. Rev. B* 83 (2011) 144418. doi:10.1103/physrevb.83.144418.
- [11] N. Barros, H. Rassam, H. Kachkachi, Microwave-assisted switching of a nanomagnet: Analytical determination of the optimal microwave field, *Phys. Rev. B* 88 (2013) 014421. doi:10.1103/physrevb.88.014421.
- [12] G. Klughertz, L. Friedland, P.-A. Hervieux, G. Manfredi, Autoresonant switching of the magnetization in single-domain nanoparticles: Two-level theory, *Phys. Rev. B* 91 (2015) 104433. doi:10.1103/physrevb.91.104433.
- [13] T. Taniguchi, D. Saida, Y. Nakatani, H. Kubota, Magnetization switching by current and microwaves, *Phys. Rev. B* 93 (2016) 014430. doi:10.1103/physrevb.93.014430.
- [14] K. Rivkin, J. B. Ketterson, Magnetization reversal in the anisotropy-dominated regime using time-dependent magnetic fields, *Appl. Phys. Lett.* 89 (2006) 252507. doi:10.1063/1.2405855.
- [15] T. Taniguchi, Magnetization switching by microwaves synchronized in the vicinity of precession frequency, *Appl. Phys. Express* 8 (2015) 083004. doi:10.7567/apex.8.083004.
- [16] J. Mögerle, R. Schuldt, J. Reiff, J. Main, R. Hernandez, Transition state dynamics of a driven magnetic free layer, *Commun. Nonlinear Sci. Numer. Simulat.* 105 (2022) 106054. doi:10.1016/j.cnsns.2021.106054.
- [17] M. Feldmaier, P. Schraft, R. Bardakcioglu, J. Reiff, M. Lober, M. Tschöpe, A. Junginger, J. Main, T. Bartsch, R. Hernandez, Invariant manifolds and rate constants in driven chemical reactions, *J. Phys. Chem. B* 123 (2019) 2070–2086. doi:10.1021/acs.jpcc.8b10541.
- [18] Y. Nagahata, R. Hernandez, T. Komatsuzaki, Phase space geometry of isolated to condensed chemical reactions, *J. Chem. Phys.* 155 (2021) 210901. doi:10.1063/5.0059618.
- [19] P. Hänggi, P. Talkner, M. Borkovec, Reaction-rate theory: Fifty years after Kramers, *Rev. Mod. Phys.* 62 (1990) 251–341. doi:10.1103/RevModPhys.62.251, and references therein.
- [20] C. Jaffé, D. Farrelly, T. Uzer, Transition state theory without time-reversal symmetry: Chaotic ionization of the hydrogen atom, *Phys. Rev. Lett.* 84 (2000) 610–613. doi:10.1103/PhysRevLett.84.610.
- [21] G. Jacucci, M. Toller, G. DeLorenzi, C. P. Flynn, Rate theory, return jump catastrophes, and the center manifold, *Phys. Rev. Lett.* 52 (1984) 295. doi:10.1103/PhysRevLett.52.295.
- [22] T. Komatsuzaki, R. S. Berry, Regularity in chaotic reaction paths. I. ar₆, *J. Chem. Phys.* 110 (1999) 9160–9173. doi:10.1063/1.478838.
- [23] T. Komatsuzaki, R. S. Berry, Chemical reaction dynamics: Many-body chaos and regularity, *Adv. Chem. Phys.* 123 (2002) 79–152. doi:10.1002/0471231509.ch2.
- [24] M. Toller, G. Jacucci, G. DeLorenzi, C. P. Flynn, Theory of classical diffusion jumps in solids, *Phys. Rev. B* 32 (1985) 2082. doi:10.1103/PhysRevB.32.2082.
- [25] A. F. Voter, F. Montalenti, T. C. Germann, Extending the time scale in atomistic simulations of materials, *Annu. Rev. Mater. Res.* 32 (2002) 321–346. doi:10.1146/annurev.matsci.32.112601.141541.
- [26] H. P. de Oliveira, A. M. Ozorio de Almeida, I. Damião Soares, E. V. Tonini, Homoclinic chaos in the dynamics of a general Bianchi type-IX model, *Phys. Rev. D* 65 (2002) 083511/1–9. doi:10.1103/PhysRevD.65.083511.
- [27] C. Jaffé, S. D. Ross, M. W. Lo, J. Marsden, D. Farrelly, T. Uzer, Statistical theory of asteroid escape rates, *Phys. Rev. Lett.* 89 (2002) 011101. doi:10.1103/PhysRevLett.89.011101.
- [28] J. Reiff, J. Zatsch, J. Main, R. Hernandez, On the stability of satellites at unstable libration points of sun–planet–moon systems, *Commun. Nonlinear Sci. Numer. Simulat.* 104 (2022) 106053. doi:10.1016/j.cnsns.2021.106053.
- [29] P. F. Bessarab, V. M. Uzdin, H. Jónsson, Harmonic transition-state theory of thermal spin transitions, *Phys. Rev. B* 85 (2012) 184409. doi:10.1103/PhysRevB.85.184409.
- [30] S. Wang, P. B. Visscher, Accelerated LLG simulation of magnetic stability: “bounce” algorithm, *IEEE Trans. Magn.* 43 (2007) 2893–2895. doi:10.1109/tmag.2007.892595.
- [31] M.-C. Ciornei, J. M. Rubi, J.-E. Wegrowe, Magnetization dynamics in the inertial regime: Nutation predicted at short time scales, *Phys. Rev. B* 83 (2011) 020410(R). doi:10.1103/PhysRevB.83.020410.
- [32] M. Fähnle, D. Steiauf, C. Illg, Generalized Gilbert equation including inertial damping: Derivation from an extended breathing Fermi surface model, *Phys. Rev. B* 84 (2011) 172403. doi:10.1103/PhysRevB.84.172403.

- [33] Y. Li, A.-L. Barra, S. Auffret, U. Ebels, W. E. Bailey, Inertial terms to magnetization dynamics in ferromagnetic thin films, *Phys. Rev. B* 92 (2015) 140413(R). doi:10.1103/PhysRevB.92.140413.
- [34] K. Neeraj, N. Awari, S. Kovalev, D. Polley, N. Z. Hagström, S. S. P. K. Arekapudi, A. Semisalova, K. Lenz, B. Green, J.-C. Deinert, I. Ilyakov, M. Chen, M. Bawatna, V. Scalera, M. d' Aquino, C. Serpico, O. Hellwig, J.-E. Wegrowe, M. Gensch, S. Bonetti, Inertial spin dynamics in ferromagnets, *Nat. Phys.* 17 (2021) 245–250. doi:10.1038/s41567-020-01040-y.
- [35] T. L. Gilbert, A phenomenological theory of damping in ferromagnetic materials, *IEEE Trans. Magn.* 40 (2004) 3443–3449. doi:10.1109/TMAG.2004.836740.
- [36] D. M. Apalkov, P. B. Visscher, Spin-torque switching: Fokker-Planck rate calculation, *Phys. Rev. B* 72 (2005) 180405(R). doi:10.1103/PhysRevB.72.180405.
- [37] C. Abert, Micromagnetics and spintronics: Models and numerical methods, *Eur. Phys. J. B* 92 (2019) 120. doi:10.1140/epjb/e2019-90599-6.
- [38] D. Steiauf, M. Fähnle, Damping of spin dynamics in nanostructures: An ab initio study, *Phys. Rev. B* 72 (2005) 064450. doi:10.1103/PhysRevB.72.064450.
- [39] M. Fähnle, D. Steiauf, Breathing Fermi surface model for noncollinear magnetization: A generalization of the Gilbert equation, *Phys. Rev. B* 73 (2006) 184427. doi:10.1103/PhysRevB.73.184427.
- [40] M. Bauer, J. Fassbender, B. Hillebrands, R. L. Stamps, Switching behavior of a Stoner particle beyond the relaxation time limit, *Phys. Rev. B* 61 (2000) 3410–3416. doi:10.1103/PhysRevB.61.3410.
- [41] J. Z. Sun, Spin-current interaction with a monodomain magnetic body: A model study, *Phys. Rev. B* 62 (2000) 570–578. doi:10.1103/PhysRevB.62.570.
- [42] J.-E. Wegrowe, M.-C. Ciornei, Magnetization dynamics, gyromagnetic relation, and inertial effects, *Am. J. Phys.* 80 (2012) 607–611. doi:10.1119/1.4709188.
- [43] T. Kikuchi, G. Tatara, Spin dynamics with inertia in metallic ferromagnets, *Phys. Rev. B* 92 (2015) 184410. doi:10.1103/PhysRevB.92.184410.
- [44] B. C. Garrett, D. G. Truhlar, Generalized transition state theory, *J. Phys. Chem.* 83 (1979) 1052–1079. doi:10.1021/j100471a031.
- [45] P. Pechukas, Transition state theory, *Annu. Rev. Phys. Chem.* 32 (1981) 159–177. doi:10.1146/annurev.pc.32.100181.001111.
- [46] E. Pollak, Periodic orbits and the theory of reactive scattering, in: M. Baer (Ed.), *Theory of Chemical Reaction Dynamics*, volume 3, CRC Press, Boca Raton, FL, 1985, p. 123.
- [47] D. G. Truhlar, B. C. Garrett, S. J. Klippenstein, Current status of transition-state theory, *J. Phys. Chem.* 100 (1996) 12771–12800. doi:10.1021/jp953748q.
- [48] W. H. Miller, Direct and correct calculation of canonical and microcanonical rate constants for chemical reactions, *J. Phys. Chem. A* 102 (1998) 793–806. doi:10.1021/jp973208o.
- [49] R. Hernandez, T. Uzer, T. Bartsch, Transition state theory in liquids beyond planar dividing surfaces, *Chem. Phys.* 370 (2010) 270–276. doi:10.1016/j.chemphys.2010.01.016.
- [50] R. Hernandez, D. Stallings, S. Iyer, The gender and urn faculty demographics data collected by oxide, in: H. N. Cheng, D. Nelson (Eds.), *Diversity in the Scientific Community Volume 1: Quantifying Diversity and Formulating Success*, volume 1255 of *ACS Symposium Series*, American Chemical Society; Oxford University Press, Washington DC, 2017, pp. 101–112. doi:10.1021/bk-2017-1256.ch006.
- [51] M. Feldmaier, R. Bardakcioglu, J. Reiff, J. Main, R. Hernandez, Phase-space resolved rates in driven multidimensional chemical reactions, *J. Chem. Phys.* 151 (2019) 244108. doi:10.1063/1.5127539.
- [52] M. Feldmaier, J. Reiff, R. M. Benito, F. Borondo, J. Main, R. Hernandez, Influence of external driving on decays in the geometry of the LiCN isomerization, *J. Chem. Phys.* 153 (2020) 084115. doi:10.1063/5.0015509.
- [53] R. Bardakcioglu, J. Reiff, M. Feldmaier, J. Main, R. Hernandez, Thermal decay rates of an activated complex in a driven model chemical reaction, *Phys. Rev. E* 102 (2020) 062204. doi:10.1103/PhysRevE.102.062204.
- [54] A. J. Lichtenberg, M. A. Liebermann, *Regular and Stochastic Motion*, Springer, New York, 1982.
- [55] R. Hernandez, W. H. Miller, Semiclassical transition state theory. A new perspective, *Chem. Phys. Lett.* 214 (1993) 129–136. doi:10.1016/0009-2614(93)90071-8.
- [56] R. Hernandez, *Application of Semiclassical Methods to Reaction Rate Theory*, Ph.D. thesis, University of California, Berkeley, CA, 1993.
- [57] S. Wiggins, L. Wiesenfeld, C. Jaffe, T. Uzer, Impenetrable barriers in phase-space, *Phys. Rev. Lett.* 86 (2001) 5478. doi:10.1103/PhysRevLett.86.5478.
- [58] T. Uzer, C. Jaffé, J. Palacián, P. Yanguas, S. Wiggins, The geometry of reaction dynamics, *Nonlinearity* 15 (2002) 957–992. doi:10.1088/0951-7715/15/4/301.
- [59] E. Ott, *Chaos in Dynamical Systems*, 2nd ed., Cambridge University Press, Cambridge, England, 2002.
- [60] S. Wiggins, The role of normally hyperbolic invariant manifolds (NHIMS) in the context of the phase space setting for chemical reaction dynamics, *Regul. Chaotic Dyn.* 21 (2016) 621–638. doi:10.1134/S1560354716060034.
- [61] C. Mendoza, A. M. Mancho, Hidden geometry of ocean flows, *Phys. Rev. Lett.* 105 (2010) 038501. doi:10.1103/PhysRevLett.105.038501.
- [62] A. M. Mancho, S. Wiggins, J. Curbelo, C. Mendoza, Lagrangian descriptors: A method for revealing phase space structures of general time dependent dynamical systems, *Commun. Nonlinear Sci. Numer. Simul.* 18 (2013) 3530 – 3557. doi:10.1016/j.cnsns.2013.05.002.
- [63] G. T. Craven, R. Hernandez, Lagrangian descriptors of thermalized transition states on time-varying energy surfaces, *Phys. Rev. Lett.* 115 (2015) 148301. doi:10.1103/PhysRevLett.115.148301.
- [64] J. Reiff, M. Feldmaier, J. Main, R. Hernandez, Dynamics and decay rates of a time-dependent two-saddle system, *Phys. Rev. E* 103 (2021) 022121. doi:10.1103/PhysRevE.103.022121.
- [65] G. T. Craven, T. Bartsch, R. Hernandez, Communication: Transition state trajectory stability determines barrier crossing rates in chemical reactions induced by time-dependent oscillating fields, *J. Chem. Phys.* 141 (2014) 041106. doi:10.1063/1.4891471.
- [66] R. Bardakcioglu, A. Junginger, M. Feldmaier, J. Main, R. Hernandez, Binary contraction method for the construction of time-dependent dividing surfaces in driven chemical reactions, *Phys. Rev. E* 98 (2018) 032204. doi:10.1103/PhysRevE.98.032204.
- [67] E. Olive, Y. Lansac, M. Meyer, M. Hayoun, J.-E. Wegrowe, Deviation from the Landau-Lifshitz-Gilbert equation in the inertial regime of the

- magnetization, *J. Appl. Phys.* 117 (2015) 213904. doi:10.1063/1.4921908.
- [68] J. Reiff, R. Bardakcioglu, M. Feldmaier, J. Main, R. Hernandez, Controlling reaction dynamics in chemical model systems through external driving, *Physica D* 427 (2021) 133013. doi:10.1016/j.physd.2021.133013.